Gold-Speckled Multimodal Nanoparticles for Noninvasive Bioimaging

Parvesh Sharma,[†] Scott C. Brown,[†] Niclas Bengtsson,[‡] Qizhi Zhang,[§] Glenn A. Walter,[||] Stephen R. Grobmyer,[⊥] Swadeshmukul Santra,[#] Huabei Jiang,[§] Edward W. Scott,[‡] and Brij M. Moudgil*,[†]

Materials Science and Engineering and Particle Engineering Research Center, Molecular Genetics and Microbiology, Biomedical Engineering, Physiology and Functional Genomics, and Department of Surgery, University of Florida, P.O. Box 116135 Gainesville, Florida 32611, and NanoScience Technology Center, Chemistry and Biomolecular Science Center, University of Central Florida, Orlando, Florida 32826

Received April 11, 2008. Revised Manuscript Received June 26, 2008

In this report the synthesis, characterization, and functional evaluation of a multimodal nanoparticulate contrast agent for noninvasive imaging through both magnetic resonance imaging (MRI) and photoacoustic tomography (PAT) is presented. The nanoparticles described herein enable high resolution and highly sensitive three-dimensional diagnostic imaging through the synergistic coupling of MRI and PAT capabilities. Gadolinium (Gd)-doped gold-speckled silica (GSS) nanoparticles, ranging from 50 to 200 nm, have been prepared in a simple one-pot synthesis using nonionic microemulsions. The photoacoustic signal is generated from a nonuniform, discontinuous gold nanodomains speckled across the silica surface, whereas the MR contrast is provided through Gd incorporated in the silica matrix. The presence of a discontinuous speckled surface, as opposed to a continuous gold shell, allows sufficient bulk water exchange with the Gd ions to generate a strong MR contrast. The dual imaging capabilities of the particles have been demonstrated through *in silicio* and *in vitro* methods. The described particles also have the capacity for therapeutic applications including the thermal ablation of tumors through the absorption of irradiated light.

Introduction

One of the important promises of nanotechnology is the development of techniques and tools for cancer diagnosis using safe, noninvasive, low-cost means with high resolution and sensitivity. Existing clinical imaging modalities, such as computed tomography, magnetic resonance imaging (MRI), positron emission tomography, and ultrasound, differ from one another in terms of detection sensitivity, spatial−temporal resolution, signal-to-noise ratio, quantitative accuracy, and long-term safety.[1,2] None of these methods are capable of providing complete structural and functional information independently.[3] Hence, it is often desirable to employ information from complimentary imaging modalities to enhance prognosis and enable early and accurate detection of tumors.[3,4] The need for complimentary diagnostic information has led to the emergence of multimodal contrast agents that are capable of generating contrast by different modalities, simultaneously.

MRI, a common clinical imaging modality, has the capability of constructing three-dimensional (3D) images of biological structures providing high anatomical details. High dosages of commercial Gd-based MR contrast agents are commonly used to improve image resolution. However, these contrast agents, by themselves, are not sensitive enough to obtain images that can be resolved at the single-cell level. Single-cell MRI capability will allow for early disease diagnosis, stem cell tracking, gene and drug delivery, etc. Therefore, the development of high-resolution image contrast agents such as nanoparticle-based MRI contrast agents has a great demand.

Photoacoustic tomography (PAT, also known as laser optoacoustic or thermoacoustic imaging) is an emerging noninvasive, nonionizing, deeply penetrating imaging modality[5,6] that combines the advantages of the sensitivity of optical methods with the resolution of diffraction-limited ultrasound. In PAT, a nonionizing short-pulsed optical laser is used as an excitation source to generate an acoustic signal resulting from thermoelastic expansion of the absorbent which is then detected and used to recover the geometry of the object. PAT has been used to image tumors,[7,8] blood

* Corresponding author. Tel.: (352) 846-1194. Fax: (352) 846-1196. E-mail: bmoudgil@perc.ufl.edu.
[†] Materials Science and Engineering and Particle Engineering Research Center, University of Florida.
[‡] Molecular Genetics and Microbiology, University of Florida.
[§] Biomedical Engineering, University of Florida.
[||] Physiology and Functional Genomics, University of Florida.
[⊥] Department of Surgery, University of Florida.
[#] NanoScience Technology Center, Chemistry and Biomolecular Science Center, University of Central Florida.

(1) Brenner, D. J.; Hall, E. J. *N. Engl. J. Med.* **2007**, *357*, 2277.
(2) Berrington de Gonzalez, A.; Darby, S. *Lancet* **2004**, *363*, 345.
(3) Cherry, S. R. *Annu. Rev. Biomed. Eng.* **2006**, *8*, 35.
(4) Babinec, P.; Babincova, M. *Med. Hypotheses* **2007**, *69*, 703.
(5) Xu, M. H.; Wang, L. H. V. *Rev. Sci. Instrum.* **2006**, *77*, 040011.
(6) Wang, L. H. V. *Dis. Markers* **2003**, *19*, 123.
(7) Esenaliev, R. O.; Karabutov, A. A.; Oraevsky, A. A. *IEEE J. Sel. Top. Quantum Electron.* **1999**, *5*, 981.
(8) Oraevsky, A. A.; Ermilov, S. A.; Conjusteau, A.; Miller, T.; Gharieb, R. R.; Lacewell, R.; Mehta, K.; Radulescu, E. G.; Herzog, D.; Thompson, S.; Stein, A.; McCorvey, M.; Otto, P.; Khamapirad, T. *Breast Cancer Res. Treat.* **2007**, *106*, S47.

10.1021/cm801020s CCC: $40.75
Published on Web 09/12/2008

vessels,[9] hemoglobin oxygenation,[10] tumor angiogenesis[11] in the absence and presence of contrast agents.[12−14] PAT provides femtomolar sensitivity and high temporal and spatial resolution.[7,9,15,16] It would be advantageous to obtain simultaneous structural and functional information with high resolution using a multimodal image contrast agent for noninvasive imaging by both PAT and MRI.

In this paper we report a novel multimodal nanoparticle that provides the first example of a single-nanoparticle contrast agent for noninvasive imaging by both PAT and MRI. The use of MRI, a well-established imaging method, in parallel with PAT (made possible through the use of these nanoparticles) is expected to enable rapid enhancement and further development of improved computational algorithms for PAT image construction—enhancing the breath and capabilities of the method. PAT may potentially prove useful for patients with cardiac pacemakers, certain metallic implants, or metallic debris (e.g., shrapnel, iron filings) in their body that are precluded from undergoing MRI scans due to strong magnetic fields. Although PAT currently does not provide the magnitude of anatomical information afforded by MRI, it can provide 3D deep tissue imagery that is comparable to MRI—particularly in the presence of contrast agents.[9,15,17] MRI−PAT bimodal contrast agents may also be used for clinical prescreening purposes to lower the burden on existing MRI facilities and provide a low-cost, nonionizing method for the analysis of soft tissue. Multimodal MRI−PAT nanoparticles are also envisaged to be potentially useful for diagnostic imaging and therapy of cancer. Because the generation of acoustic signal is due to the thermoelastic expansion of the PAT contrast agents, it is possible to elevate the temperature of the target tissue by increasing the intensity of the incident laser beam, causing significant damage to tumor tissue. Thus, the development of safer, nonionizing diagnostic methods would enable implementation of advanced bioimaging solutions for larger spectrum of patients that can be applied in the field, in common clinics, as well as in major hospitals and medical institutions.

Materials and Methods

Materials. Tetraethylorthosilicate (TEOS), Triton X-100 (TX-100), *n*-hexanol, 3-(aminopropyl)triethoxysilane (APTS), and cyclohexane were purchased from Aldrich Chemical Co. Inc. *N*-(Trimethoxysilyl-propyl)ethyldiaminetriacetic acid trisodium salt (TSPETE) (45% wt % solution in water) was purchased from Gelest Co., gold chloride, gadolinium acetate, and hydrazine hydrate were obtained from Acros Organics, and ammonium hydroxide (NH_4OH, 28−30 wt %) was obtained from the Fisher Scientific Co. All other chemicals were of analytical reagent grade. Deionized (DI) water (NANOpure, Barnstead) was used for the preparation of all solutions.

Methods. *Synthesis of Gd-Doped GSS Nanoparticles.* The complete synthesis of the multimodal nanoparticles was done in one pot using reverse micelles. The water-in-oil (W/O) microemulsion was prepared by mixing TX-100 cyclohexane, *n*-hexanol (1: 4.2:1 v/v), and appropriate water. *n*-Hexanol was used as a cosurfactant to the nonionic surfactant, TX-100. An amount of 0.050 mL of TEOS was added in the beginning to the microemulsion and allowed to equilibrate for 30 min. The hydrolysis and polymerization of TEOS was then initiated by adding 0.05−0.200 mL of NH_4OH. The overall W_0 (water to surfactant molar ratio) after addition of NH_4OH was 10. After allowing silica polymerization reaction to go for 24 h, the surface of the silica nanoparticle was modified with the addition of 0.025 mL of TSPETE and 0.050 mL of TEOS. The resulting solution was allowed to stir overnight. This was followed by the addition of 0.10 mL of 0.1 M Gd(III) acetate solution and stirring for another 4 h. This was followed by addition of 0.5 mL of 0.25 M $HAuCl_4$, prepared in degassed water, and 1.1 M solution of reducing agent (hydrazine hydrate). The solution was allowed to stir for ∼12 h. The progress of the reaction at each step was monitored by UV−vis absorption spectroscopy. The Gd-doped GSS nanoparticles were then isolated from the microemulsion by adding 5 mL of 200 proof ethanol. The solution was then stirred for a few minutes. This led to the complete breakdown of reverse micelles with the formation of two immiscible layers of aqueous ethanol and cyclohexane. The nanoparticles along with the surfactant molecules were accumulated in bottom ethanol layer. The top layer of cyclohexane was carefully removed, and the particles were centrifuged. The particles were washed three times with ethanol and five times with water in order to completely remove surfactant molecules. Each centrifugation step, during washing was followed by vortexing and sonication to redisperse the pelleted particles. After complete removal of surfactant the particles were redispersed in Nanopure water to obtain a concentration of ca. 2 mg/mL for further characterization.

Particle Size Measurements. The particle size and distribution were measured by dynamic light scattering (DLS) using a Microtrac NANOTRAC and CPS disk centrifuge. The size and morphology of the particles were determined by transmission electron microscopy (TEM). TEM and energy-dispersive X-ray spectroscopy (EDS) spectra of the particles were done using JEOL 2010F transmission electron microscope.

Inductively Coupled Plasma Experiments. Inductively coupled plasma (ICP) measurements were performed using a Perkin-Elmer Plasma 3200 system equipped with two monochromators covering the spectral range of 165−785 nm with a grated ruling of 3600 lines/mm. Briefly, 0.050 g of the nanoparticle sample was digested using aqua regia solution. [**Caution***:* Aqua regia digestion should be performed with care in a hood. Its reaction with GSS nanoparticles produces acrid and toxic fumes.] Au and Gd were completely solubilized in the aqua regia, whereas the silica matrix was settled at the bottom of the container as a white powder. After complete digestion the solution was filtered to separate the silica particles as residue. The particles were washed three times with aqua regia solution and finally twice with nanopure water. The filtrate and the particles were all collected together and boiled to concentrate the volume to 15.0 mL. After instrument calibration was performed for Au and Gd estimation, the filtrate was analyzed by ICP for quantitative estimation of Gd and Au.

(9) Wang, X.; Pang, Y.; Ku, G.; Xie, X.; Stoica, G.; Wang, L. V. *Nat. Biotechnol.* **2003**, *21*, 803.
(10) Wang, X.; Xie, X.; Ku, G.; Wang, L. V.; Stoica, G. *J. Biomed. Opt.* **2006**, *11*, 024015.
(11) Ku, G.; Wang, X.; Xie, X.; Stoica, G.; Wang, L. V. *Appl. Opt.* **2005**, *44*, 770.
(12) Eghtedari, M.; Oraevsky, A.; Copland, J. A.; Kotov, N. A.; Conjusteau, A.; Motamedi, M. *Nano Lett.* **2007**, *7*, 1914.
(13) Wang, X.; Ku, G.; Wegiel, M. A.; Bornhop, D. J.; Stoica, G.; Wang, L. V. *Opt. Lett.* **2004**, *29*, 730.
(14) Wang, Y. W.; Xie, X. Y.; Wang, X. D.; Ku, G.; Gill, K. L.; O'Neal, D. P.; Stoica, G.; Wang, L. V. *Nano Lett.* **2004**, *4*, 1689.
(15) Ku, G.; Wang, X.; Stoica, G.; Wang, L. V. *Phys. Med. Biol.* **2004**, *49*, 1329.
(16) Ku, G.; Fornage, B. D.; Jin, X.; Xu, M. H.; Hunt, K. K.; Wang, L. V. *Technol. Cancer Res. Treat.* **2005**, *4*, 559.
(17) Ku, G.; Wang, L. V. *Opt. Lett.* **2005**, *30*, 507.

MR Phantom Preparation for Relaxivity Measurements. All MRI measurements were recorded using a 4.7 T Bruker Avance MR scanner. Phantom preparation for MR relaxivity measurements was done by serially diluting a 10 mg/mL stock solution of Gd-doped GSS nanoparticles with ddH_2O and mixing with a 1% agarose solution (Ultra-Pure agarose, Invitrogen, Carlsbad, CA) yielding a final concentration of 0.5% agarose. The resulting nanoparticle concentrations of 5, 2.5, 1.25, 0.625, and 0.3125 mg/mL were then injected into 100 μL capillary tubes (Curtin-Matheson Scientific, Broomall, PA) and allowed to solidify on ice, thereby eliminating sedimentation during relaxivity measurements. The comparison of MR response between Gd-doped GSS nanoparticles and silica nanoparticles (without any gold or Gd) was performed similarly by diluting 10 mg/mL nanoparticles in 1% agarose solution (Supporting Information). Control phantoms containing just 0.5% and 1% agarose were simultaneously imaged to determine effect of agarose on relaxation times. Right before imaging, all samples were placed together inside a water-filled FACS tube (BD Falcon, Franklin Lakes, NJ) to avoid susceptibility artifacts from the surrounding air.

MR Relaxivity for Gd-Doped GSS Nanoparticles. All relaxivity data were analyzed using Paravision software (PV3.02; Bruker Medical). For measuring T_1 relaxation times, axial spin−echo (SE) scan sequences were obtained with TE = 4.5 ms, matrix size = 128 × 128, FOV = 2.8 × 2.8 cm^2, spectral width = 180 kHz, one average, 1 mm slice thickness, and varying TR values of 11, 6, 3, 1.5, 0.75, 0.5, 0.25, 0.125, 0.075, 0.05, 0.025, and 0.015 s. For T_2 relaxation measurements, axial T_2-weighted single-slice multiecho images were obtained with TR = 11 s, TE = 5 ms ΔTE = 5 ms (60 echoes), matrix size = 128 × 128, FOV = 2.8 × 2.8 cm^2, spectral width = 100 kHz, two signal averages, and a 1 mm slice thickness. T_1 and T_2 maps were calculated assuming a monoexponential signal decay and by using a nonlinear function, least-squares curve fitting on the relationship between changes in mean signal intensity within a region of interest (ROI) to TR and TE. T_1 and T_2 relaxation times(s) for the Gd-doped GSS nanoparticles in 0.5% agarose were then derived by ROI measurements of the test samples converted into R_1 and R_2 relaxation rates ($1/T_{1,2}$ (s^{-1})). Finally, $R_{1,2}$ values were plotted against the concentration of Gd on the nanoparticle and r_1 and r_2 (mM^{-1} s^{-1}) relaxivities were obtained as the slope of the resulting linear plot.

T_2* relaxivity measurements were acquired by T_2*-weighted FLASH gradient echo scan sequences. TRs were kept constant at 500 ms with varying TEs of 4, 8, 12, 16, 20, 40, 60, and 100 ms, FOV = 2.8 × 2.8 cm^2, matrix size = 256 × 256, two signal averages, spectral width = 60 kHz, and 1 mm slice thickness. Image J software (NIH) with an MR analysis calculator plug-in was used to quantify T_2* values by stacking the individual FLASH sequences with varying TEs and creating a T_2* map. ROIs for each cell sample were then drawn to contain the entire cross section of each of the samples, and values were then plotted as R_2* (or the inverse of T_2* ($1/T_2$*, (s^{-1}))), against the concentration of Gd in the sample (Excel, Microsoft Inc.). R_2* relaxivity (mM^{-1} s^{-1}) was later obtained as the slope of the resulting linear plot. Data are presented as the mean ± SD of measurements.

PAT Instrumentation. A mechanical scanning photoacoustic system with single acoustic transducer to collect the acoustic signals was utilized. A schematic representation of the PAT experimental setup is shown in the Supporting Information. A pulsed Nd:YAG laser (Altos, Bozeman, MT) working at 532 nm with 4 ns pulse duration, 10 Hz repetition rate and 360 mJ maximum pulse power acted as light source. The diameter of laser beam was expanded to 30 mm by a lens. An immersion acoustic transducer with 1 MHz nominal frequency (Valpey Fisher, Hopkinton, MA) was driven by a motorized rotator to receive acoustic signals over 360° for phantoms at an interval of 3°, and thus a total of 120 measurements were performed for one planar scanning. The scanning plane could be adjusted along the z-axis by mounting the rotator and the transducer on a platform driven by a linear stage. The acoustic transducer was immersed into the water tank while the phantom was placed at the center of the tank where it was illuminated by the laser. The complex wave field signal was amplified by a pulser/receiver (GE Panametrics, Waltham, MA) and then acquired by a high-speed PCI data acquisition board. PAT images were reconstructed by our reconstruction algorithm that is based on the finite element solution to the photoacoustic wave equation in the frequency domain, which can provide stable inverse solutions.[18] Phantoms for imaging were constructed using intralipid, India ink, distilled water, and 2% agar powder as described previously.[19] The diameters of all phantoms used in this study were 25 mm. The absorption and reduced scattering coefficients (optical properties) of these phantoms were 0.007 and 0.5 mm^{-1}, respectively. Nanoparticles were embedded in the phantom at a depth of 2 mm for imaging.

Macrophage Labeling and Phantom Preparation for MRI and PAT. Mouse monocyte/macrophage J774 cells were defrosted, resuspended in Dulbecco's modified Eagle's medium (DMEM) (GIBCO, Grand Island, NY) supplemented with 10% fetal bovine serum (Summit Biotechnology, Ft. Collins, CO), 1% glutamax (GIBCO), 1% penicillin/streptomycin (GIBCO), and incubated at a density of 5 × 10^5 cells/mL in 100 mm culture dishes at 37 °C and 5% CO_2. Media was replaced 24 h after plating, and the cells were allowed to attach and grow to confluency (usually within 2−3 days). Old media was replaced with fresh before the cells were harvested and washed twice by spinning them down at 1100 rpm for 5 min using a Sorvall RT7 plus ultracentrifuge and resuspending in fresh DMEM complete media. Cells were subsequently replated at a density of 2 × 10^5 and again allowed to attach and grow to confluency. Cells were passaged for 3−4 times before the start of the labeling experiment. During labeling, 1 × 10^6 freshly split J774 cells/mL DMEM complete were incubated overnight with 100 μg/mL of Gd-doped GSS nanoparticles in a six-well tissue culture dish. The next day label-containing media was aspirated off and replaced by fresh media before labeled and unlabeled control cells were scraped up, washed twice in ice-cold Dulbecco's phosphate-buffered saline (DPBS) (GIBCO, Grand Island, NY), counted, and resuspended at a density of 3.33 × 10^7 cells/mL each in DPBS (2 × 10^6 cells in 60 μL DPBS). Cells were kept on ice until the time of imaging when 20 μL of cell suspension was then injected in the phantom. The same phantom was used for MRI and PAT experiments in succession.

MRI Measurements on J774 Cells Labeled with Gd-Doped GSS Nanoparticles. The sample phantom containing GSS-labeled J774 and control cells was placed inside a solenoid coil and imaged at 4.7 T magnetic field strength. T_1- and T_2-weighted SE scan sequences were used to detect Gd on the nanoparticles inside the cells. For generating T_1-weighted images a multislice multiecho (MSME) pulse sequence was used with TR = 500 ms, TE = 5 ms, matrix size = 256 × 256, FOV = 3 × 3 cm^2, spectral width = 100 kHz, two signal averages, and a 1 mm slice thickness. T_2-weighted images was acquired either by using a MSME pulse sequence with TR = 500 ms, TE = 100 ms, matrix size = 256 × 256, FOV = 3 × 3 cm^2, spectral width = 100 kHz, two signal averages, and a 1 mm slice thickness or by using a rapid acquisition with relaxation enhancement (RARE) pulse sequence with TR =

(18) Yuan, Z.; Wu, C. F.; Zhao, H. Z.; Jiang, H. B. *Opt. Lett.* **2005**, *30*, 3054.
(19) Tam, A. C. *Rev. Mod. Phys.* **1986**, *58*, 381.

1000 ms, TE = 12 ms, matrix size = 256 × 256, FOV = 3 × 3 cm^2, spectral width = 60 kHz, four signal averages, RARE factor = 8, and a 1 mm slice thickness.

Results and Discussion

Existing contrast agents for PAT include near-IR absorbing dyes and gold-based nanomaterials,[12,17,20] which have been demonstrated for various therapeutic and imaging applications.[21−26] Although the possibility of using gold nanoshells as exogenous PAT contrast agent has been described,[27] only a few experimental reports exist in the literature.[14] Similarly, the application of molecular dyes in PAT has been limited due to their poor *in vivo* stability and rapid clearance from the biological systems.[28] Although gold nanoshells exhibit the desired optical and photothermal properties for PAT, the need for a continuous shell of up to 20 nm in thickness (resulting in an overall particle size of 120−150 nm[21,27,29]) limits their capacity to internally integrate MRI contrast through the restriction of water exchange. Moreover, their larger size (>120 nm) could limit certain bioimaging applications such as tracking stem cells, viruses, etc., where size tunability, in particular, smaller particle size, is preferred.

To overcome the size restrictions of existing gold nanoshell particles as well as introduce the property of being multimodal contrast agents, we have developed a gold−silica hybrid material termed gold-speckled silica (GSS) nanoparticles. These MRI−PAT-active multimodal nanoparticles have a surface layer composed of discontinuous, irregular gold nanodomains of varying crystallinity that are incorporated within the pores and on the exterior of the supporting silica matrix. The multitude of dielectric−metal interfaces created by this method gives rise to unique photothermal properties that enable the use of these materials as contrast agents in PAT. Gd incorporated in the silica matrix of the nanoparticles provides MRI contrast. These multimodal GSS nanoparticles possess high MRI relaxivity and at the same time produce a strong PAT contrast.

The complete synthesis of the multimodal GSS nanoparticles has been carried out in one pot using the nonionic W/O microemulsion method. The synthesis procedure for these nanoparticles has been described in detail in the Materials and Methods. Briefly, Gd-doped silica nanoparticles are first formed by cocondensation of TEOS and a silane reagent that strongly chelates polyvalent metal ions[30−34] (TSPETE) in the water core of the TX-100/*n*-hexanol/water W/O microemulsion. Incorporation of chloroauric acid followed by its reduction was the carried out within the surface layer of the silica nanoparticles. By manipulating W_0 of the microemulsions and the reactant concentrations, we were able to tune Gd-doped GSS nanoparticle size from less than 50 to 200 nm. Parts A and B of Figure 1 show representative TEM micrographs for two different samples prepared at W_0 10 and 14, depicting mean particle size of ∼100 (±10) and 55 (±5) nm, respectively. GSS nanoparticles up to 200 nm and larger were synthesized at W_0 5 (Supporting Information) using the same microemulsion system. The particle sizes were confirmed using DLS and disk centrifuge techniques.

A key difference between the current particles and those previously described in the literature lies in the nature of the gold nanoparticle generation and deposition on and in the silica matrix. In a traditional synthesis route (seed-mediated synthesis), 1−2 nm uniform gold nanoparticles are first deposited on the silica surface as small clusters. In the following step, gold nanoshell is created by allowing further deposition and growth of these gold clusters. The shell thickness of the gold nanoshells can vary between 1−20 nm. Unlike the traditional approach of depositing gold nanoparticles[21,27] onto silica nanoparticles, we incubated Gd-doped silica nanoparticle within the aqueous core of the microemulsion with chloroauric acid, allowing gold ions to permeate further into the mesoporous silica matrix. Upon reduction a unique gold-speckled surface results due to the deposition of the gold nanodomains. Via this method discontinuous, randomly deposited, sometimes templated, and often irregular gold nanoclusters are formed within and on the surface of the silica core. High-resolution TEM (HR-TEM) micrographs of ∼100 nm Gd-doped GSS nanoparticles (prepared at $W_0 = 10$) demonstrate speckled surface deposits of gold, as seen in areas of darker contrast on the silica surface (Figure 1C) and as areas of lighter contrast in the dark-field TEM picture (Figure 1D). Note that Gd doping also contributes to the background as a darker and lighter haze in Figure 1, parts C and D, respectively. The HRTEM micrograph (Figure 2) shows scattered deposition of gold nanoparticles ranging from less than 1 to 5 nm, with varying crystallinity, on the silica surface. These random and irregular clustered deposits, which include templated deposits within the mesopores, make this class of particles distinct and provide for their unique optical properties such as efficient photothermal properties. Since these particles were also doped with Gd ions—a paramagnetic species that affects the longitudinal relaxation rate of water—they exhibited MRI contrast.

(20) Yang, X.; Skrabalak, S. E.; Li, Z. Y.; Xia, Y.; Wang, L. V. *Nano Lett.* **2007**, *7*, 3798.
(21) Halas, N. *MRS Bull.* **2005**, *30*, 362.
(22) Shi, W. L.; Sahoo, Y.; Swihart, M. T.; Prasad, P. N. *Langmuir* **2005**, *21*, 1610.
(23) Liu, Z. X.; Song, H. W.; Yu, L. X.; Yang, L. M. *Appl. Phys. Lett.* **2005**, *86*, 113109.
(24) Park, H. Y.; Schadt, M. J.; Wang, L.; Lim, I. I.; Njoki, P. N.; Kim, S. H.; Jang, M. Y.; Luo, J.; Zhong, C. J. *Langmuir* **2007**, *23*, 9050.
(25) Hirsch, L. R.; Stafford, R. J.; Bankson, J. A.; Sershen, S. R.; Rivera, B.; Price, R. E.; Hazle, J. D.; Halas, N. J.; West, J. L. *Proc. Natl. Acad. Sci. U.S.A.* **2003**, *100*, 13549.
(26) Loo, C.; Lowery, A.; Halas, N.; West, J.; Drezek, R. *Nano Lett.* **2005**, *5*, 709.
(27) Hirsch, L. R.; Gobin, A. M.; Lowery, A. R.; Tam, F.; Drezek, R. A.; Halas, N. J.; West, J. L. *Ann. Biomed. Eng.* **2006**, *34*, 15.
(28) Kim, G.; Huang, S. W.; Day, K. C.; O'Donnell, M.; Agayan, R. R.; Day, M. A.; Kopelman, R.; Ashkenazi, S. *J. Biomed. Opt.* **2007**, *12*, 044020.
(29) Oldenburg, S. J.; Westcott, S. L.; Averitt, R. D.; Halas, N. J. *J. Chem. Phys.* **1999**, *111*, 4729.
(30) Bringley, J. F.; Lerat, Y. J. United States Patent Applications 2004-868626, 2005276862, AN 2005:1311129, 2005.
(31) Bringley, J. F.; Patton, D. L.; Wien, R. W.; Lerat, Y. J. F. United States Patent Applications 2004-936910, 2005226913, AN 2005: 1103187, 2005.
(32) Bronstein, L. M.; Linton, C. N.; Stein, B. D.; Dixit, S.; Svergun, D. I. *Abstr. Pap.—Am. Chem. Soc.* **2004**, *228*, U501.
(33) Santra, S.; Bagwe, R. P.; Dutta, D.; Stanley, J. T.; Walter, G. A.; Tan, W.; Moudgil, B. M.; Mericle, R. A. *Adv. Mater.* **2005**, *17*, 2165.
(34) Yang, H. S.; Santra, S.; Walter, G. A.; Holloway, P. H. *Adv. Mater.* **2006**, *18*, 2890.

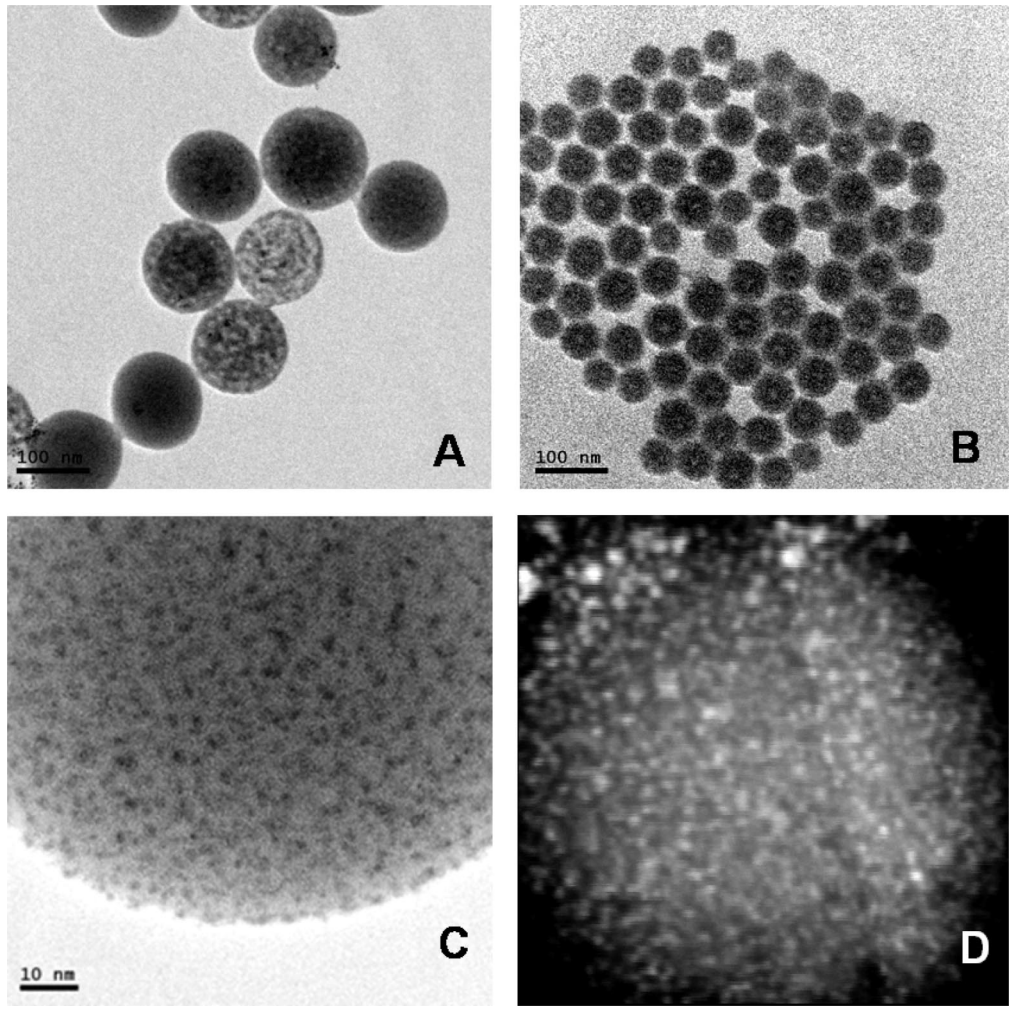

Figure 1. (A) Representative TEM picture of Gd-doped GSS nanoparticles, with an average size of ~100 nm and (B) Gd-doped GSS particles with an average size of ~50 nm. (C) High-resolution TEM picture of the nanoparticle showing the presence of electron-dense gold on the silica nanoparticle and (D) dark-field TEM picture showing the contrast from the presence of the electron-dense species.

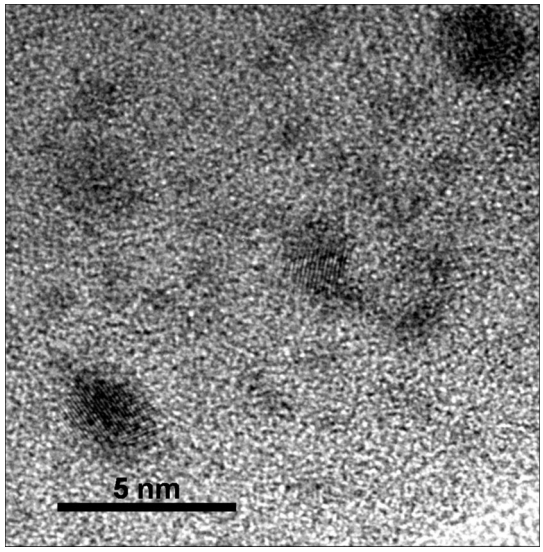

Figure 2. High-resolution TEM picture of the nanoparticle showing the lattice planes of gold nanoparticles as deposited on the silica nanoparticle.

The elemental composition of the Gd-doped GSS nanoparticles particles was determined using EDS and ICP techniques. A representative line scan (Figure 3A) and composite EDS spectrum (Figure 3B) showed the spectral counts corresponding to Si, O, Au, Gd, and the overall spectrum for the nanoparticle, respectively. The elemental composition as determined by ICP gave average number of atoms of Au and Gd to be ~426 200 and ~34 000 per nanoparticle, respectively. Theoretical calculations showed that ~72 times more number of gold atoms would be present in a single gold nanoparticle of similar dimension. To our knowledge, this is the first report of one-pot synthesis of Gd-doped GSS nanoparticulate contrast agents as well as the first example of a multimodal contrast agent for MRI and PAT. The evaluation of the MRI and PAT bifunctional properties of these nanoparticulates has been demonstrated using agar gel phantoms as described in the following sections.

The Gd-doped GSS nanoparticles were shown to generate MR contrast on both T_1 and T_2 proton relaxation time weighted sequences as depicted in Figure 4, parts A and B. Quantitatively, MR contrast is evaluated by estimating the relaxivity of the nanoparticle. The relaxivity (R_i, $i = 1, 2$) is defined as the gradient of the linear plot of relaxation rates ($1/T_i$, $i = 1, 2$) versus Gd concentration [Gd],[35] i.e., $1/T_i = 1/T_o + R_i[\mathrm{Gd}]$, where T_i is the relaxation time for a contrast

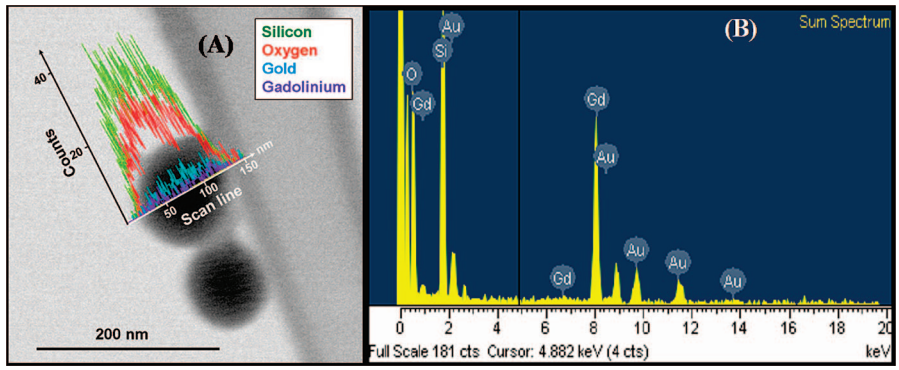

Figure 3. (A) Line scan of Gd-doped GSS nanoparticle showing the spectral emission from the constituent elements. (B) EDS spectrum of the multimodal nanoparticles showing the presence of silicon (Si), oxygen (O), gold (Au), and gadolinium (Gd).

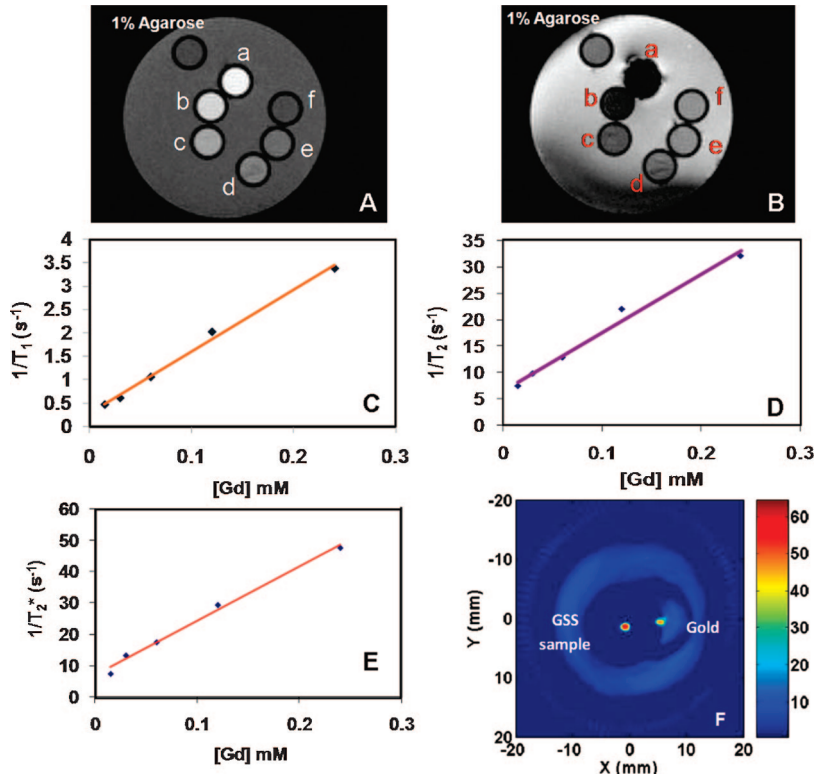

Figure 4. Magnetic resonance data and PAT contrast from Gd-doped GSS nanoparticle. (A) T_1-weighted (repetition time (TR) = 11 000 ms, echo time (TE) = 4.2 ms) and (B) T_2* TR = 500 ms, TE = 40 ms images of serial dilutions of Gd-doped GSS nanoparticle: (a) 0.24, (b) 0.12, (c) 0.06, (d) 0.03, and (e) 0.015 mM of Gd in 0.5% agarose and (f) 0.5% agarose (as control). Linear plots of Gd concentration vs (C) $1/T_1$, (D) $1/T_2$, and (E) $1/T_2$*, respectively, to obtain ionic relaxivities, R_1, R_2, and R_2*, respectively, of Gd-doped GSS nanoparticle. (F) Comparison of PAT contrast from gold and GSS nanoparticles of similar size and concentration (8 μL of 10 mg/mL) in a tissue-like phantom with background: absorption coefficient $\mu a = 0.007$ mm^{-1} and reduced scattering coefficient, $\mu s' = 0.5$ mm^{-1}. A stronger photo-acoustic signal is obtained from GSS nanoparticles as compared to gold nanoparticles.

agent solution concentration [Gd] and T_o is the relaxation time in the absence of a contrast agent. From the data in Figure 4C−E, the relaxivities R_1, R_2, and R_2* are determined to be 13, 110, and 173 mM^{-1} s^{-1}, respectively. When compared with commercially available contrast agents, Gd−GSS exhibit much higher relaxivity values under the same magnetic strength of 4.7 T.[36] In MRI, it is well-established that the Gd-generated MR contrast relies on the relaxation process of the water molecules in association with the Gd ion and those exchanged in the surrounding environment.[37,38] For an efficient relaxation process, rapid water exchange between bound (or inner coordination water) with the bulk water and slow tumbling play an important role.[37] The Gd-doped GSS nanoparticles address both these factors. First, the presence of the discontinuous GSS surface allows sufficient bulk water exchange with the Gd ions enabling MR tracking ability. It should be noted that a continuous gold shell over the silica core could limit the extent of water exchange inhibiting T_1 contrast. Second, tumbling rate—another important factor for producing an effective MRI contrast—is also reduced in the Gd-doped GSS particles through the rigid binding of Gd to the nanoparticle

(35) Toth, E.; Bolskar, R. D.; Borel, A.; Gonzalez, G.; Helm, L.; Merbach, A. E.; Sitharaman, B.; Wilson, L. J. *J. Am. Chem. Soc.* **2005**, *127*, 799.
(36) Rohrer, M.; Bauer, H.; Mintorovitch, J.; Requardt, M.; Weinmann, H. J. *Invest. Radiol.* **2005**, *40*, 715.
(37) Aime, S.; Botta, M.; Terreno, E. *Adv. Inorg. Chem.* **2005**, *57*, 173.
(38) Caravan, P. *Chem. Soc. Rev.* **2006**, *35*, 512.

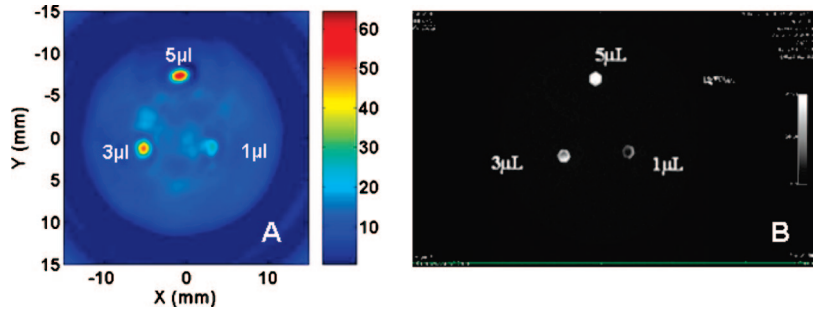

Figure 5. (A) The PAT and (B) MRI (T_1) contrast from the same phantom, using 1, 3, and 5 μL (particle concentration, 10 mg/mL) of Gd-doped GSS using sample in tissue-like phantom with background absorption coefficient $\mu a = 0.007$ mm^{-1} and scattering coefficient, $\mu s' = 0.5$ mm^{-1}, demonstrating the multimodal nature of the nanoparticles.

surface. Because the tumbling rates are mass-dependent, nanoparticles are much slower than free Gd chelates and thus produce an enhanced relaxation. One of the major limitations of current molecular chelates used as MR contrast agent is their low sensitivity; this requires the use of higher dosages and results in poor targetability.[38] Both these concerns are also addressed in the present construct. Approximately, 34 000 ions of Gd are captured per nanoparticle with an average size of 100 nm, which is higher than the number of Gd ions previously reported in other nanoparticles such as synthetic polymers (6−70 ions) and in dendrimers (between 5 and 1331 ions, strongly dependent on particle size[39]) and comparable to perfluorocarbon nanoparticles (90 000 Gd ions in 250 nm diameter particle[40]).

The ability of Gd−GSS nanoparticles to generate photoacoustic contrast was confirmed by placing the particles in an agar phantom containing India ink and intralipid to simulate tissue-like absorption and scattering. Figure 4F shows the comparison of PAT contrast from GSS nanoparticles and compares it to that of similar size and concentration of gold nanoparticles. The dark red region in the area of the nanoparticles, with respect to the blue background, demonstrates that a strong PAT contrast is observed from the particles. As shown in Figure 4F the GSS nanoparticles generated a stronger photoacoustic signal when compared to the gold nanoparticles. The stronger PAT contrast from the GSS nanoparticles, in spite of the presence of ~72-fold less gold atoms, demonstrates them as a better PAT contrast agent. Control experiments were also performed using silica nanoparticles (without gold or Gd) which illustrated that the bare silica nanoparticles do not have a significant PAT contrast (Supporting Information). Because the PAT originates from the optical absorption of the illuminating laser wavelength, the GSS particles also hold therapeutic potential for the thermal ablation of tumors. Hence, the particles described here hold both multimodal imaging as well as therapeutic capabilities.

To evaluate the bimodal character of the GSS nanoparticles, simultaneous MR and photoacoustic evaluation was carried out. To achieve this, the GSS particles were placed in tissue-like phantom. The phantom was imaged for PAT and MR in succession, and the results are shown in Figure

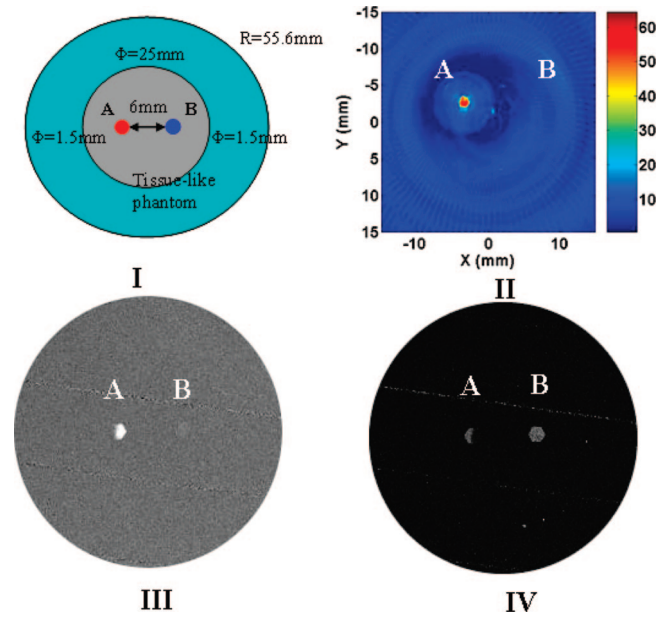

Figure 6. Panel I shows the position of J 774 macrophage cells labeled with GSS nanoparticles marked as A, and unlabeled cells B, in the tissue-like phantom. Panel II shows the PAT image, panel III is the T_1-weighted spin−echo image with TR = 500 ms, TE = 6 ms, and panel IV is the T_2-weighted spin−echo image with TR = 500 ms, TE = 100 ms.

5. An increase in the MR and PAT signal intensity is observed with increasing particulate amounts.

In vitro studies have also been carried out with the GSS nanoparticles to assess the functional ability of the particles in the cellular environment. The uptake of the GSS nanoparticles by J774 macrophages was carried out as explained in the Materials and Methods. The cells were then placed in tissue-like phantom and imaged by PAT and MRI in succession. Figure 6 shows the phantom design with the sample placement and the MR and PAT images obtained with the same phantom. It is observed that the cells labeled with the GSS nanoparticles produce a strong PAT contrast as compared to the background. The MR image of the same phantom shows the ability to generate the T_1 and T_2 contrast. The in vitro experiments demonstrated the capability of the GSS nanoparticles to generate an efficient PAT and MR contrast in living cells, showing potential use of GSS nanoparticles as in vivo cell tracker.

In summary, we have described the synthesis and systematic characterization of new MRI- and PAT-active multimodal nanoparticle-based contrast agents. The nano-

(39) Caravan, P.; Ellison, J. J.; McMurry, T. J.; Lauffer, R. B. *Chem. Rev.* **1999**, *99*, 2293.
(40) Morawski, A. M.; Winter, P. M.; Crowder, K. C.; Caruthers, S. D.; Fuhrhop, R. W.; Scott, M. J.; Robertson, J. D.; Abendschein, D. R.; Lanza, G. M.; Wickline, S. A. *Magn. Reson. Med.* **2004**, *51*, 480.

particles were prepared using a W/O microemulsion method where the nanoparticle size was tuned by varying microemulsion parameters such as W_0 value and reactant concentration. The composite nanoparticles are composed of a silica core containing chelated Gd moieties, partially covered with randomly deposited irregular gold speckles, or nanoclusters. The speckled surface permits efficient water exchange between the Gd in the nanoparticle and the bulk water, resulting in an efficient MR contrast. In addition the particles also generate an efficient PAT contrast emanating from metal−dielectric interfaces. These multimodal nanoparticles have the potential to be used as diagnostic as well as therapeutic agents.

Acknowledgment. The authors acknowledge the financial support of the Particle Engineering Research Center (PERC) at the University of Florida, the National Science Foundation (NSF Grant EEC-94-02989, NSF-NIRT Grant EEC-0506560, National High Field Magnet Laboratory), the National Institutes of Health (Grants 1-P20-RR020654-01, RO1HL75258, R01HL78670), James & Esther King Biomedical Research Program (Grant 06NIR-05), Patricia Adams Cancer Nanotechnology Research Fund, and the Industrial Partners of the PERC for support of this research. Any opinions, findings, and conclusions or recommendations expressed in this material are those of the author(s) and do not necessarily reflect those of the National Science Foundation. The authors thank Kerry Siebein at the Major Analytical Instrumentation Center (MAIC) of the University of Florida for assistance in high-resolution transmission electron microscopy measurements. NMR (MRI) data were obtained at the Advanced Magnetic Resonance Imaging and Spectroscopy (AMRIS) facility in the McKnight Brain Institute of the University of Florida. P.S. acknowledges Principal, St. Stephen's College, Delhi, India for granting leave for research.

Supporting Information Available: Additional information is provided regarding the synthesis of larger GSS nanoparticles, a typical extinction spectra of GSS, the PAT experimental setup, as well as a comparison of MR and PAT properties with silica nanoparticles (PDF). This material is available free of charge via the Internet at http://pubs.acs.org.

CM801020S